Journal of
MATERIALS RESEARCH

Aging of the Inconel 718 alloy between 500 and 750 °C

C. Slama
Laboratoire de Structure des Matériaux Métalliques, Université de Paris-Sud, Bâtiment 414, 91405 Orsay Cedex, France

C. Servant
Laboratoire de Métallurgie Structurale, URA CNRS 1107, Université de Paris-Sud, Bâtiment 414, 91405 Orsay Cedex, France

G. Cizeron
Laboratoire de Structure des Matériaux Métalliques, Université de Paris-Sud, Bâtiment 414, 91405 Orsay Cedex, France

(Received 13 October 1996; accepted 27 January 1997)

The aging of the NC 19 Fe Nb alloy (Inconel 718), previously quenched from 990 °C, is characterized by a hardness peak at 650 °C, then a maximum in hardness at about 750 °C. Over this temperature, the hardness progressively decreases. In the 550–650 °C temperature range, TEM observations have revealed that β (Ni_3Nb) precipitates are formed as long platelets parallel between them within the same grain, as well as extremely fine $\gamma'[Ni_3(Ti, Al)]$ particles responsible for the observed improvement in hardness. For a tempering temperature higher than 650 °C, a first hardening occurs after a 4 h treatment, which has been associated with the γ' phase precipitation, with a more or less spherical shape. Beyond this time, a second hardening takes place linked to the γ'' phase precipitation (Ni_3Nb, bct $D0_{22}$ structure), as thin platelet shaped, perfectly coherent with the matrix. The misfit between the γ and γ'' phases is about 3% in the $\langle 001\rangle\gamma''$ direction and lower than 1% in the $\langle 100\rangle\gamma''$ and $\langle 010\rangle\gamma''$ directions. During a longer aging at 750 °C, the γ'' platelets progressively dissolve while β precipitates grow.

I. INTRODUCTION

Inconel 718 is a nickel-base superalloy largely used in the fabrication of critical pieces for turbine engines because of its high mechanical properties (yield strength up to 650 °C, impact strength and fracture toughness down to −40 °C), as well as good corrosion resistance. In addition, this alloy can be easily forged and welded.

Paulonis *et al.*[1] showed that the strengthening phase in the alloy 718 is a metastable body-centered tetragonal ($D0_{22}$ γ'' phase (Ni_3Nb). This phase is long, disk-shaped, and lies parallel to the {100} planes of the matrix. The crystalline structures of the γ'' precipitates and the γ phase are related as follows:

$$(011)\gamma''\|\{001\}\gamma \quad \text{and} \quad \langle 100\rangle\gamma''\|\langle 100\rangle\gamma\,.$$

These authors have also shown the existence of a small amount of a γ' phase $Ni_3(T, Al)$ (fcc $L1_2$ structure), appearing as a fine dispersion, of quasispherical particles which are coherent with the γ matrix. The role of the γ' phase is also strengthening, but to a lesser degree than the γ'' precipitates (the volume fraction of γ'' being, as a matter of fact, 4 times bigger than that of γ'). After treatment at temperatures equal to or higher than 750 °C, the particle size of the γ'' phase increases rapidly, then these precipitates start to dissolve at the advantage of a stable orthohombic ($D0_a$) $\beta-Ni_3Nb$ phase: this change induces an overaging of the alloy and some brittleness. (The β phase is sometimes called δ in certain publications.)

According to nuances of 718 alloy the Al at. %/Ti at. % ratio is between 0.8 and 1.75, whereas the Al + Ti/Nb ratio can vary between 0.65 and 0.9 (contents likewise expressed in at. %).

According to Sundararaman *et al.*,[6–18] the strengthening γ' and γ'' precipitates are formed simultaneously in the 550–600 °C temperature range for long-time aging; at the opposite, they are formed—always simultaneously—in the temperature range of 700 °C to 900 °C for short-time aging. We must, however, note that these conclusions of the above-mentioned authors concern an alloy of such a composition that the Al + Ti/Nb ratio is equal to 0.66; in fact, in the case of alloys presenting a value of this ratio higher than 0.8, Cozar and Pineau[19] have shown that the γ' phase precipitation precedes the γ'' phase precipitation. Also, Marsh[4] noted that the

TABLE I. Chemical composition of alloy 718 (upper table: wt. %; lower table: at. %).

Ni	Fe	Cr	Nb + Ta	Mo	Ti	Al	Co	Si	Mn	Cu	Ca	Mg	Pb	C	B	S	P
52.94	19.22	17.94	5.11	2.95	0.93	0.53	0.14	0.04	0.04	<0.10	<0.002	<0.003	<0.001	0.034	<0.005	<0.002	0.009

Ni	Fe	Cr	Nb	Mo	Ti	Al	Ti + Al/Nb	Ti/Al
52.58	20.06	20.10	3.20	1.79	1.13	1.14	0.71	0.99

precipitation of the γ' phase took place before that of the γ'' phase in the temperature range of 780 to 820 °C.

Moreover, in the case of long-duration aging and in the interval 700–900 °C we observe, in addition, the formation of the β phase[6–18]; that phase becomes major if the treatments are carried out in the 900–1000 °C temperature range. This β phase does not contribute significantly to the hardening of the alloy; on the contrary, it seems to have a beneficial effect on stress rupture ductility. The earlier formation of metastable γ' and γ'' phases (in relation to the β phase) has been attributed to the difference of the lattice mismatches which are weaker in the case of the γ/γ' or γ/γ'' interfaces than in that of the γ/β interface.

In this work, we have been mainly interested in the study of the precipitates resulting from an isothermal aging performed after quenching, as well as in the identification of the phases responsible for the different stages of hardening. On the other hand, by using x-ray diffraction techniques, we have calculated the values of the lattice parameters and the misfits between, respectively, the γ'', γ' phases and the γ matrix.

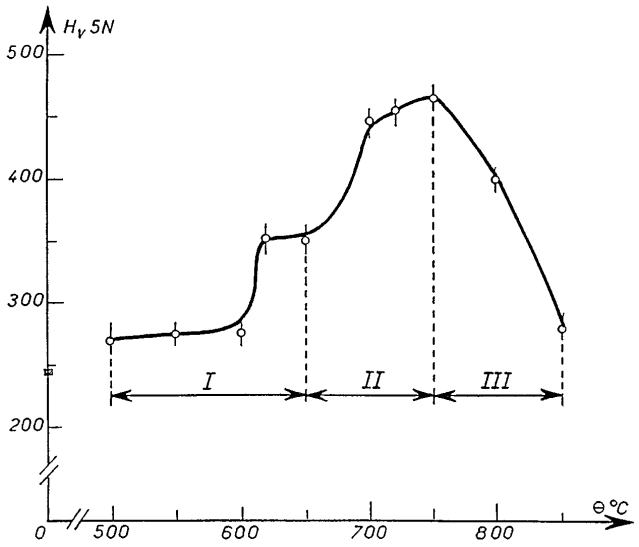

FIG. 1. Isochronal hardness curves as a function of temperature (aging time: 4 h).

II. MATERIAL AND EXPERIMENTAL METHODS

The composition of the nickel-base superalloy 718 is given in Table I. The alloy was supplied by the Acieries Aubert et Duval, as a circular bar having a diameter of 68 mm and a length of 170 mm. After rolling, the heat treatments performed on this bar were as follows: 960 °C/1 h/air cooled + 720 °C/8 h/furnace cooled at 50 °C per hour to 620 °C/8 h/air cooled.

The study of the aging, after isochronal and/or isothermal tempering, was carried out with the following methods:

(i) Vickers hardness tests performed with a Shimadzu apparatus under a load of 5 N. Each value plotted represents the mean value over ten measurements.

(ii) X-ray diffraction analysis carried out with a D 501 type Siemens diffractometer by using Cu K_α radiation (except when noted differently) and working in the following conditions: (V = 30 kV, I = 24 mA). X-ray diffraction experiments were also performed on precipitates electrolytically extracted from the heat-treated specimens. The solution used for the extraction of precipitates consisted of 10 vol. % of HCl in methanol (V = 220 mV, extraction time = 5 to 6 h). The extracted precipitates are dried before the x-ray diffraction examination. The extraction of the precipitated phases is rather difficult for a tempering temperature lower than or equal to 550 °C. Indeed, in this temperature range, a dissolution duration higher than 12 h is required in order to obtain a sufficient residue quantity for the x-ray diffraction analysis.

(iii) TEM examinations were carried out with the help of 200 C and 2000 EX JEOL microscopes (the latter operating at 200 kV and equipped with a tilt rotation probe holder). After the aging treatment, the samples were mechanically ground to ~100 μm thickness, then electropolished in a Struers twin-jet unit at 0 °C in a bath containing 10 cm^3 perchloric acid and 90 cm^3 ethylic alcohol, under 19 V.

(iv) Before every test, all the specimens were annealed for 30 min at 990 °C in a vertical furnace under an argon atmosphere (oxygen content <10 ppm), then water quenched. The specimens were than aged at different temperatures ranging from 500 to 750 °C, and finally water quenched.

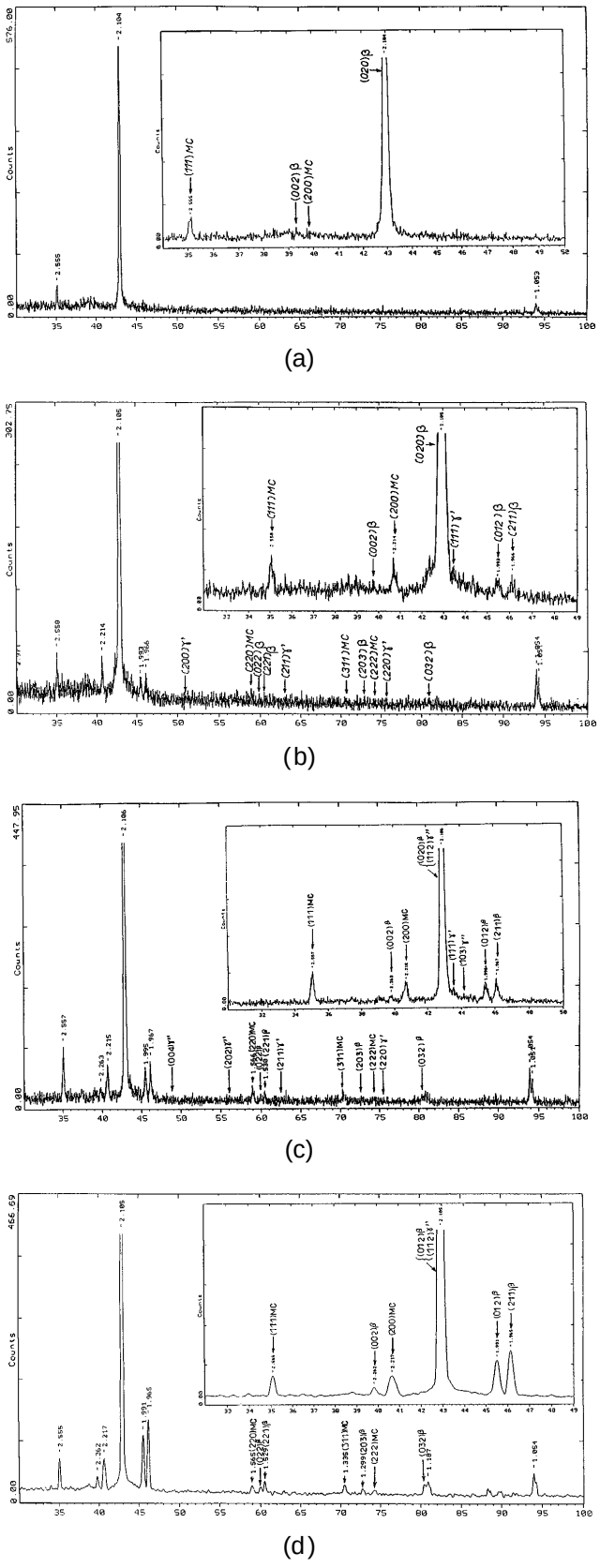

FIG. 2. X-ray diffraction patterns obtained from the extraction residues at (a) 550 °C, (b) 650 °C, (c) 750 °C, and (d) 850 °C.

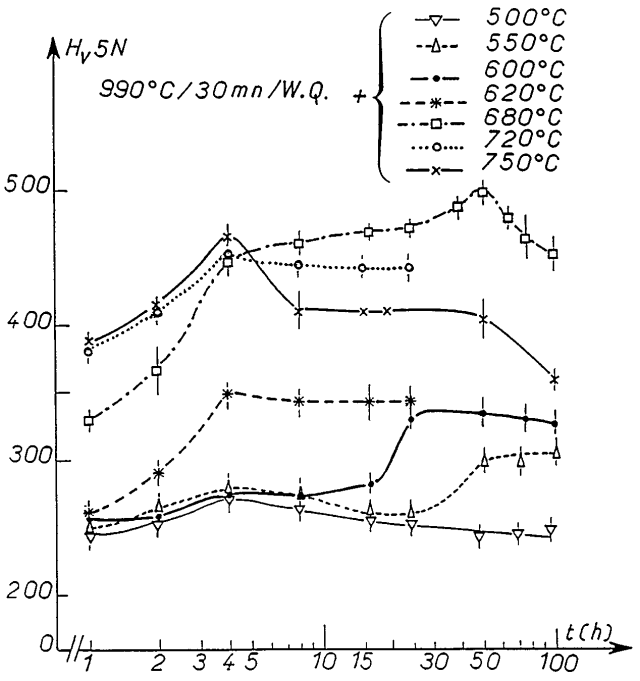

FIG. 3. Isothermal hardness curves as function of aging temperature.

III. EXPERIMENTAL RESULTS

A. Isochronal tempering

The specimens first homogenized for 30 nm at 990 °C, then water quenched, were submitted to a 4 h isochronal tempering at various temperatures ranging from 500 to 850 °C. The 990 °C temperature was chosen because after heating to such a temperature, no β lamella is detected[2] (or at least its residual quantity is very low). Anyway, these values (990 °C/30 nm) were similar to those mentioned in the literature. When Basile and Radavich[3] studied the tempering behavior of 718 alloy, they homogenized their specimens for 15 nm at 1000 °C before undergoing a water quench. According to Marsh[4] and Radavich,[3] the β phase as a small quantity in grain boundaries has a major importance in limiting the grain growth.

1. Hardness evolution

Figure 1 gives the hardness evolution as a function of the θ_R tempering temperature (for a t_R duration equal to 4 h). Three ranges of temperature may be distinguished:

Range I: 500–650 °C. Between 500 and 600 °C, the hardness does not vary and is equal to 275 HV; the hardness, previously measured on samples quenched from 990 °C, was equal to 245 HV. Nevertheless, between 600 and 650 °C, a rapid increase of this mechanical property

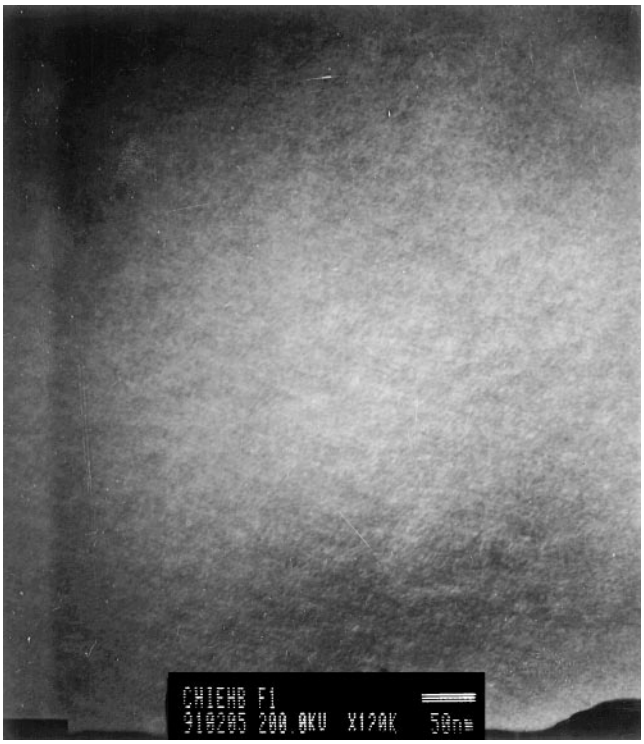

(a)

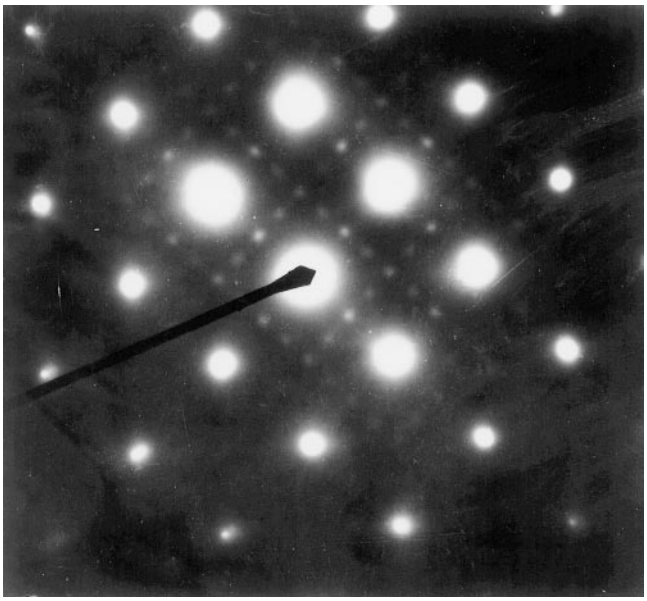

(b)

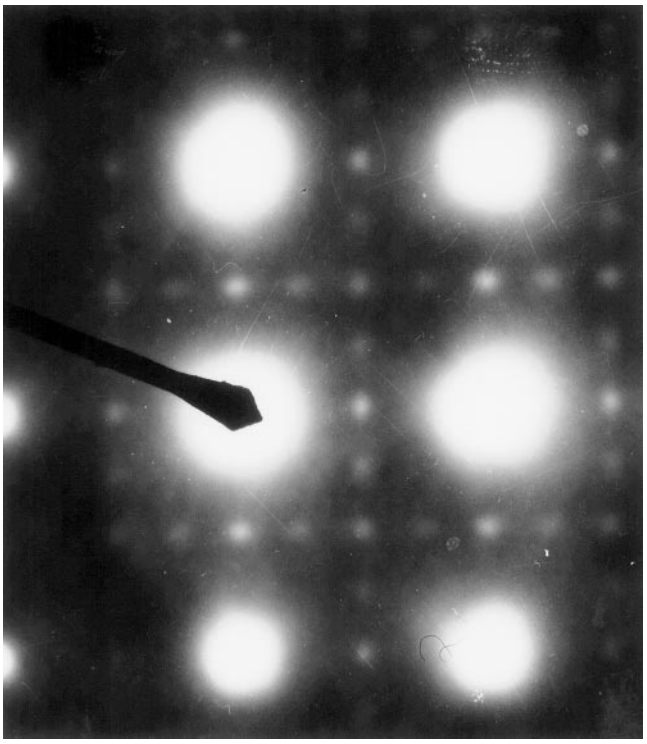

(c)

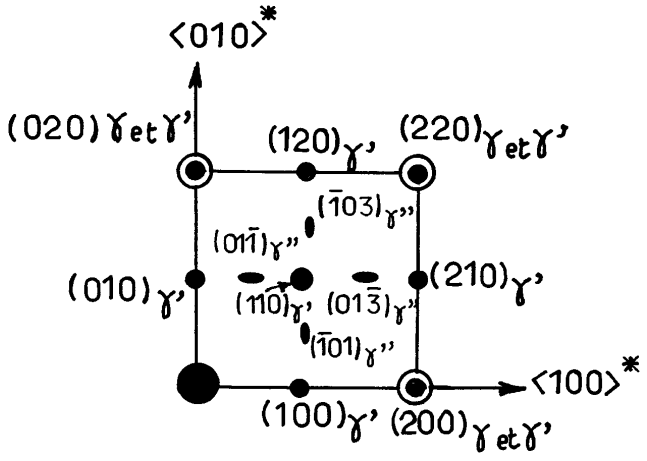

(d)

FIG. 4. Alloy aged for 50 h at 550 °C: (a) bright field, (b) electron diffraction pattern with the ⟨001⟩γ zone axis, (c) higher magnification of this diffraction pattern, and (d) schematic representation of (c).

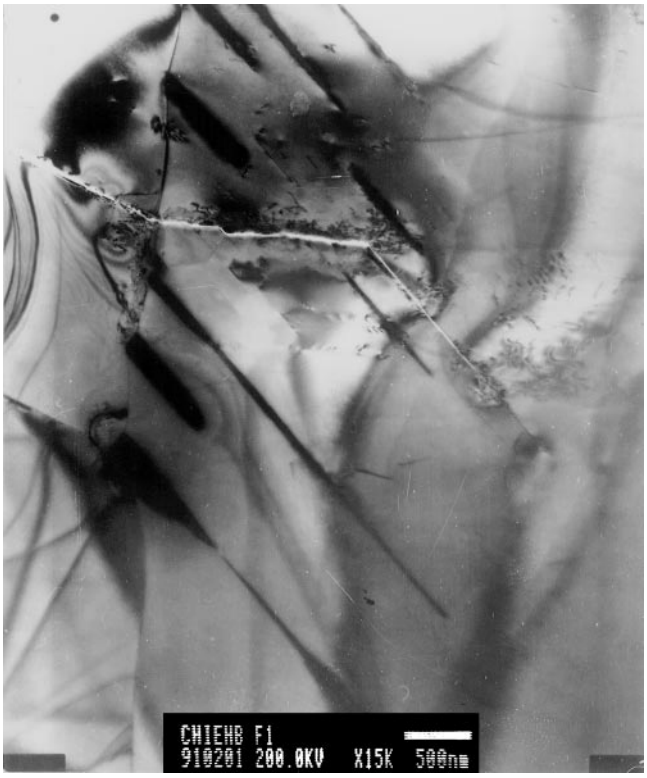

(a)

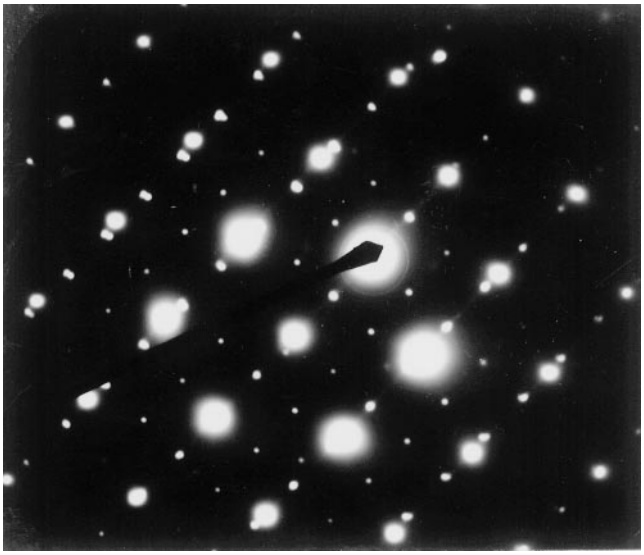

(b)

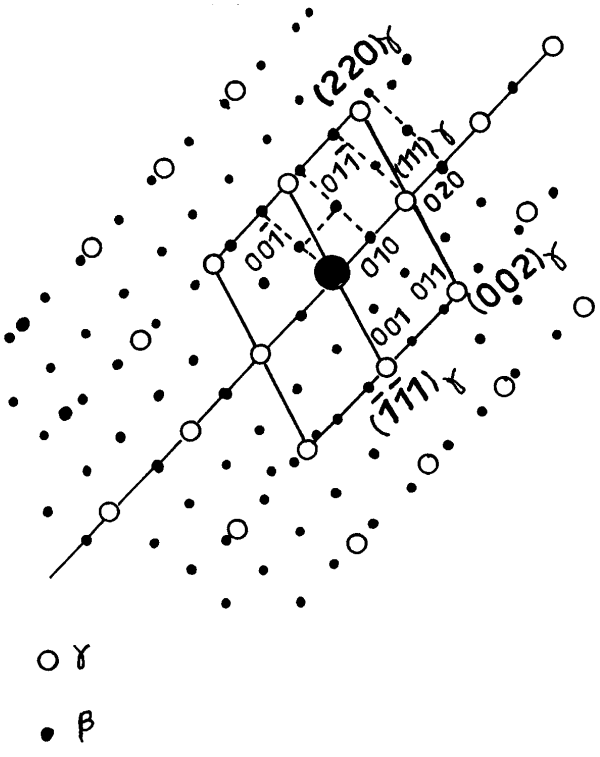

(c)

FIG. 5. Alloy aged for 50 h at 550 °C showing the morphology of the β platelets: (a) bright field and (b, c) electron diffraction patterns showing that the $\langle \bar{1}10 \rangle \gamma$ and $\langle 100 \rangle \beta$ zone axes are parallel.

(a)

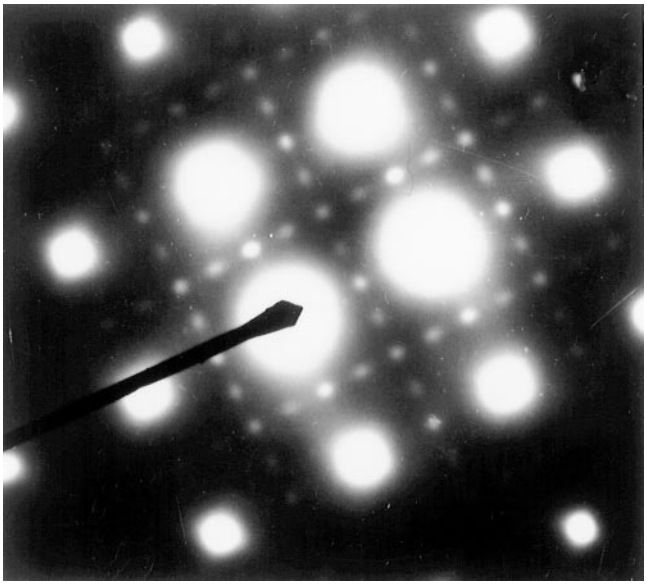

(b)

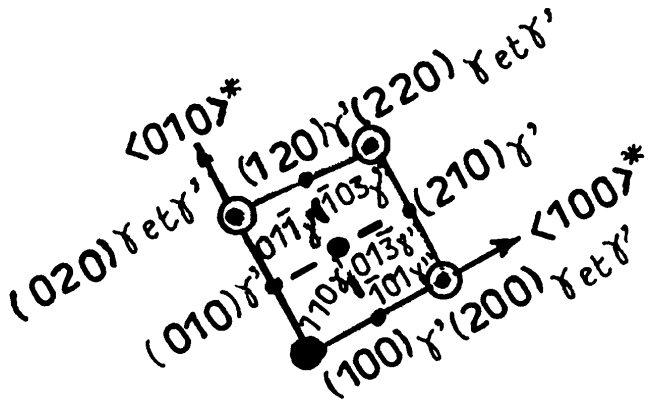

(c)

FIG. 6. Tempering from 24 h at 600 °C: (a) bright field, (b) electron diffraction pattern with the $\langle 001 \rangle \gamma$ zone axis, and (c) schematic representation.

is observed: after tempering at 650 °C the hardness value is 350 HV.

Range II: 650–750 °C. A noticeable increase in hardness is observed; the maximum hardness is obtained for $\theta_R = 750$ °C and is equal to 466 HV.

Range III: 750–850 °C. For temperatures $\theta_R > 750$ °C, the hardness diminishes as θ_R increases; this decrease is maximum when $\theta_R > 800$ °C. The hardness varies from 400 HV (4 h/800 °C) down to 280 HV (4 h/850 °C).

2. Identification of precipitates by x-ray diffraction

This identification was done on the base of patterns recorded from electrolytic extraction residues, the phase determination being based on ASTM files.

FIG. 7. Alloy aged for 24 h at 600 °C showing the β platelets growing within the γ grain.

After aging at 550 °C, the following lines (as a function of the increasing angle 2θ) were identified: (Nb, Ti)C {111}, β {002}, (Nb, Ti)C {200}, and β {020} [Fig. 2(a)].

After aging at 650 °C, the {111}, {200}, {211}, and {220} peaks of the γ' phase (fcc $L1_2$ structure) are observed [Fig. 2(b)]. One can conclude that the hardening observed in Fig. 1 is due to the γ' phase precipitation.

After treatment at 750 °C [Fig. 2(c)], in addition to the previous precipitates, the presence of supplementary peaks associated with the γ'' phase, is noted, i.e., {112}, {103}, {004}, {202} peaks. The resulting hardness after such a treatment (HV = 466) is linked to the precipitation of the γ'' (Ni_3Nb) phase with a body-centered tetragonal structure.

Moreover, the γ' phase is no longer observed after treatment at 850 °C; the progressive disappearance of the {103}, {004}, and {202} peaks of the γ'' phase after tempering at this temperature is also noted [Fig. 2(d)].

In addition, an important increase of β phase intensities is noted in comparison with those observed after tempering at 750 °C; this means that a growing of the β particles has occurred by subtracting niobium from the surrounding γ'' phase. These phenomena produce a progressive decrease in hardness (Fig. 1) which is only 280 HV after treatment at 850 °C.

However, for short-time aging, we should remember that proving, by x-ray diffraction, the presence of the γ' phase or the γ'' phase is very difficult; these phases cannot be distinguished very well from the background. Nevertheless, the electron diffraction patterns corresponding to the treatments (550 °C/50 h, 600 °C/24 h, and 750 °C/4 h) reveal the presence of the spots of the γ' and γ'' phases. This leads us to think that the weak intensity x-ray diffraction lines, existing in the above-discussed x-ray diffraction patterns, correspond very probably to the γ' and γ'' precipitates.

B. Isothermal tempering

Different specimens were submitted to isothermal tempering in a temperature range from 500 to 750 °C; this temperature range was determined from the dilatometric behavior of a specimen in the quenched state submitted to a continuous heating. Indeed, during heating, two successive contractions are observed[2]: the first one occurs between 485 and 640 °C and is associated with the simultaneous precipitation of β and γ' phases; the second one occurs between 640 and 760 °C, as the γ'' phase precipitation occurs.

1. Hardness change

Figure 3 shows the hardness change as a function of the tempering duration at different temperatures.

For temperatures $\leqslant$620 °C, the hardening generally occurs after an incubation period. The incubation time at 600 is shorter than at 550 °C, and it is almost nil at 620 °C.

This incubation period and hardening kinetics depend on the diffusion rate of some of the alloying elements such as Al, Ti, and Nb which are present in γ', γ'', and β precipitated phases. At low temperatures (500–600 °C), the diffusion rate is weak and the precipitation occurs rather slowly; consequently, an incubation time is observed and the highest observed hardness is equal only to about 330 HV, even after a 30–50 h tempering.

At 680 °C, the temperature is sufficiently high to allow the diffusion to be operative and to induce a rapid strengthening; consequently, the volume fraction of precipitates will be more important and the maximum value will be higher (HV = 500). Furthermore, it is stressed that the hardening takes place in two successive steps (the second starting only after 20 h of tempering).

At 750 °C, the diffusion rate is still higher and the hardening kinetics is faster, in such a way that after a 4 h tempering at this temperature the hardness is equal to 465. But the coarsening of precipitates leads rapidly to

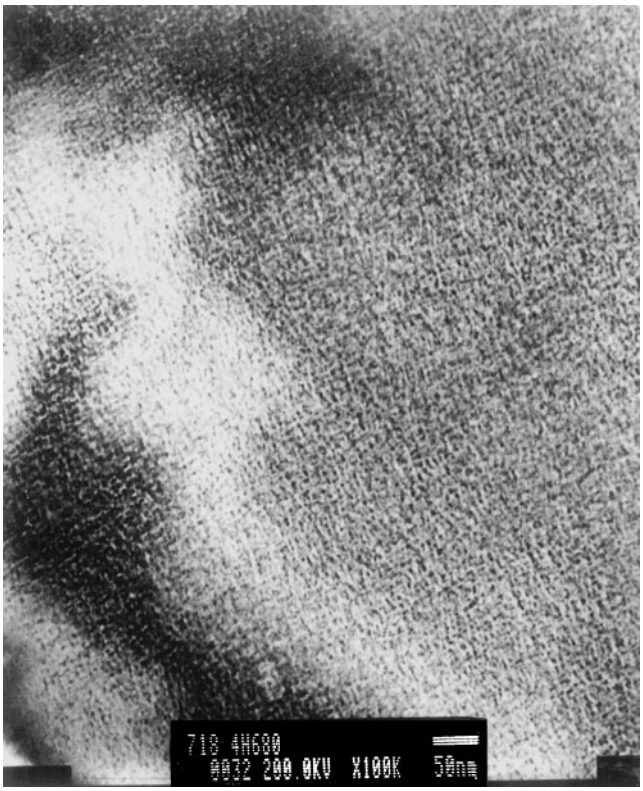

(a)

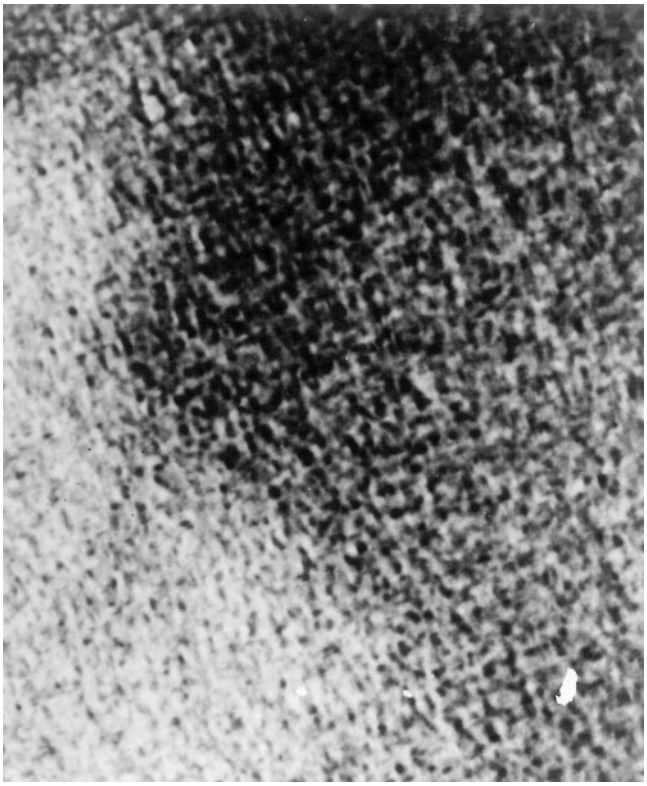

(b)

FIG. 8. Tempering for 4 h at 680 °C. Precipitation outset of γ'' and γ' phases: (a) bright field and (b) higher magnification of the same zone, 240,000×.

a hardness decrease, the more important as the duration of the isothermal soaking has been long.

2. Nature and morphology of precipitates

TEM examinations were made on thin foils heat-treated at different temperatures and in structural states for which the hardness presents particular values.

Aging at 550 and 600 °C

Bright-field observation of a sample aged at 550 °C for 50 h [Fig. 4(a)] shows a matrix with a uniform and very fine precipitation. The corresponding diffraction pattern [Fig. 4(b)] shows spots of $\langle 001\rangle\gamma$ zone axis of the matrix plus superlattice spots. Observation with a higher magnification of this diffraction pattern [Fig. 4(c)] distinguishes two types of superlattice spot: (i) The first are more intense and round-shaped, some of them being localized at half distance from the matrix spots, others being merged with them. The spot in the center of the elementary unit cell of the matrix can be indexed as one of the γ' fcc phase with the $L1_2$ structure [Fig. 4(d)]. Indeed, controversies still exist concerning the sequence of formation of the γ'' and γ' phases.[3] (ii) The others have weaker intensities and lie along the $\langle 100\rangle^*\gamma$ and $\langle 010\rangle^*\gamma$ directions. Their identification [Fig. 4(d)] shows that they belong to the γ'' phase.

After the same treatment (50 h at 550 °C), the observed β phase is shown on Fig. 5. These precipitates appear as long platelets, parallel within the same grain, and growing from the grain boundaries toward the center. The formation of the β precipitates seems to come under a cellular precipitation mechanism starting from the γ grain boundaries. According to Kirman,[5] precipitation of the β phase at low temperature can occur by a cellular mechanism at the γ boundaries or inside the grains at higher temperatures ($\geqslant$750 °C). In this last case, Sundararaman[6] has shown that the β phase precipitates in the twin boundaries for a long time of aging. On Fig. 5(a), it can also be seen that the interface between two γ grains is not straight but exhibits—in the neighborhood of β precipitates—some curvature which has been previously described by Tu and Turnbull.[7,8]

The β phase platelets are parallel to {111} matrix planes and the following relationships have been

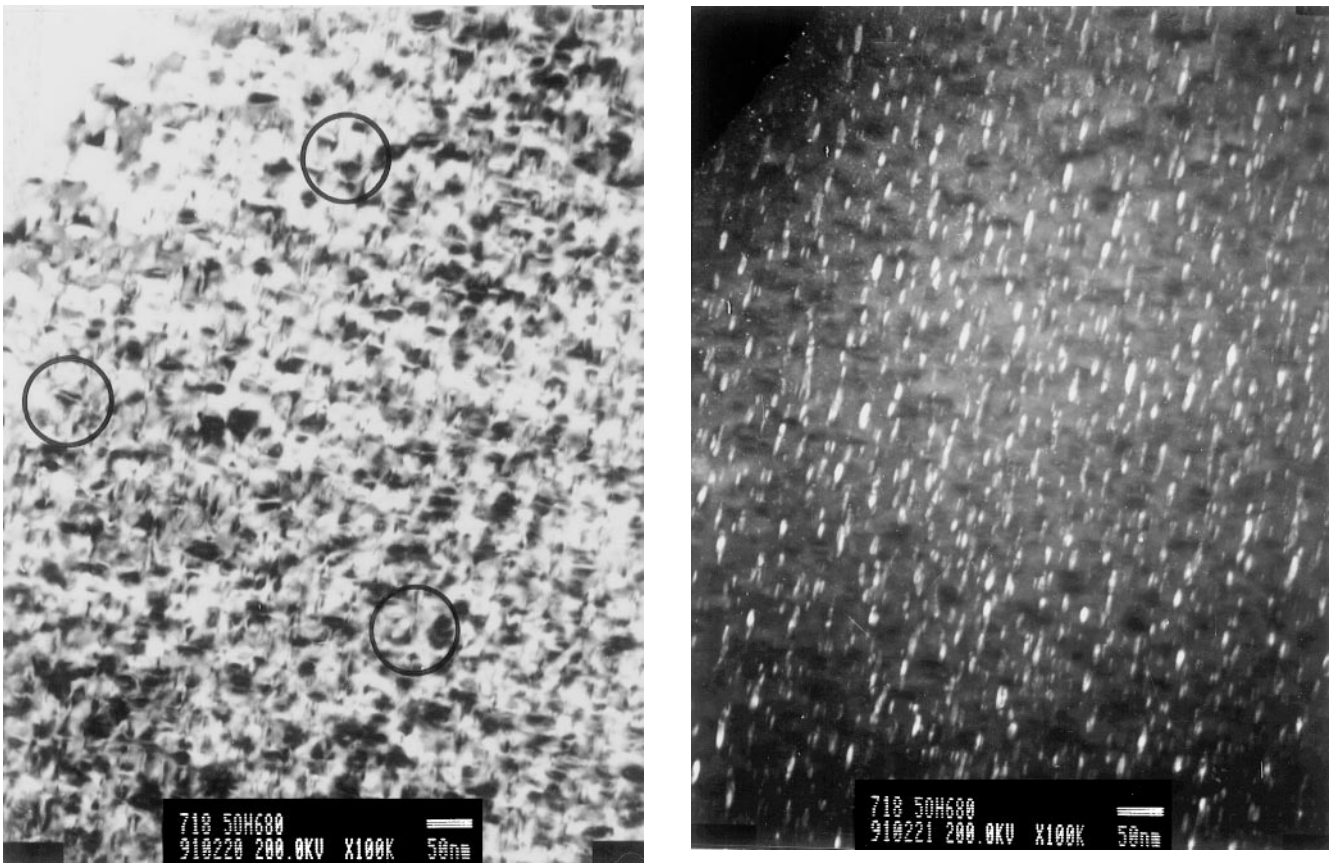

FIG. 9. Alloy aged for 50 h at 680 °C: (a) bright-field micrograph showing the precipitation morphology of γ'' and γ' phases, (b) dark-field micrograph using $(1\bar{1}0)\gamma''$ spot, and (c, d) electron diffraction pattern with zone axis $\langle 1\bar{1}0\rangle\gamma \parallel \langle 1\bar{1}0\rangle\gamma''$.

determined [Fig. 5(b)]:

$$\{010\}\beta \| \{111\}\gamma$$
$$\langle 100\rangle\beta \| \langle \bar{1}10\rangle\gamma\,.$$

The same relationships have already been found by Kirman.[5]

Figure 6(a) is relative to a sample treated for 24 h at 600 °C; it shows that the precipitation is still very fine and homogeneous in the matrix. The diffraction pattern of the matrix [Fig. 6(b)] is similar to that of Fig. 4(b): superlattice spots of γ'' and γ' phases are observed with the matrix spots. Here again γ' spots are slightly more intense than those of γ''. This can be interpreted by the more important γ' volume fraction than that of γ'' when tempering at 550 or 600 °C. In addition, after a 24 h treatment at 600 °C, it can be seen in Fig. 7 that in the γ grain, the β platelets begin to coalesce and form slightly thicker plates which are also longer than the ones resulting from a 50 h treatment at 550 °C. A cellular mechanism is still operating from the γ grain boundary.

Aging at 680 °C

After a 4 h treatment at 680 °C an increase of hardness (HV5N $\sim$ 450) is observed which results from an important precipitation of very fine and evenly distributed particles (Fig. 8) with a two type contrast in bright field: A long double-lobe contrast associated with the coherent γ'' phase and a "butterfly" one (much weaker) associated with the coherent spherical γ' particles. The γ' phase is responsible for the observed hardening, because after 4 h of aging at 680 °C (Fig. 18), the x-ray diffraction lines {111}, {211}, and {220} associated with the γ' phase are observed.

A sample treated for 50 h and 680 °C shows a very abundant precipitation of the γ'' phase. On a bright-field micrograph [Fig. 9(a)] the γ'' plates appear with a double-lobe contrast while the γ' spherical precipitates

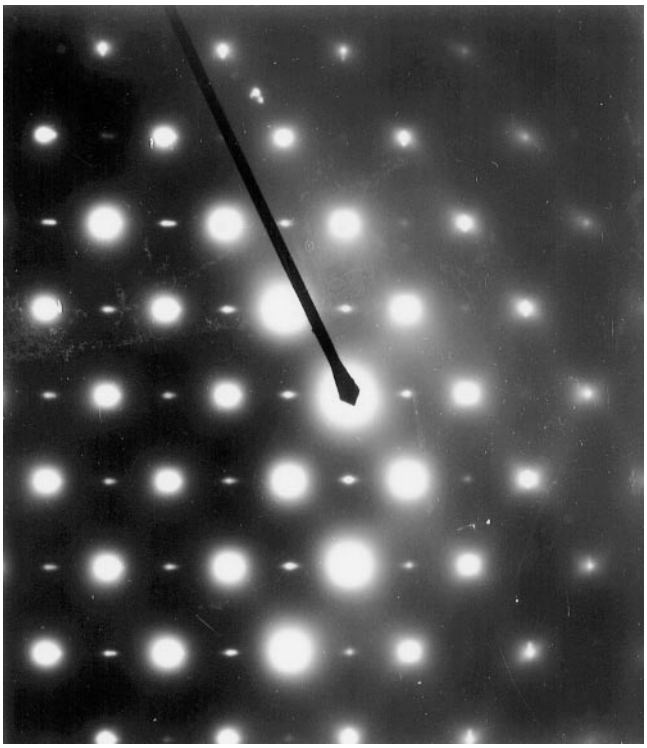

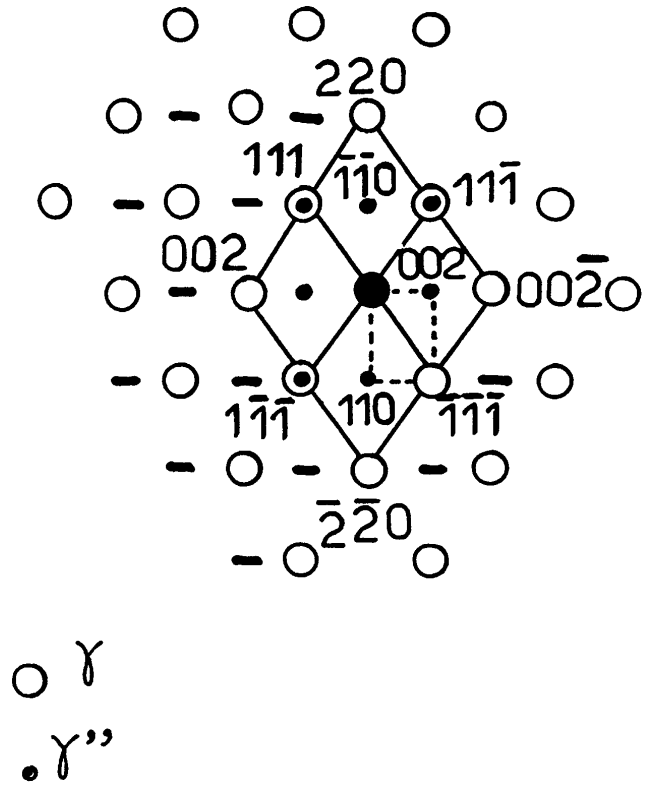

(c) (d)

FIG. 9. (*continued from previous page*)

cannot be identified by their contrast. On a dark-field micrograph—obtained from a $(\bar{1}10)\gamma''$ spot—long γ'' precipitates of the same family are lightened [Fig. 9(b)]. Moreover, at the tip of these γ'' precipitates, some small γ' spherical precipitates may be observed. Indeed, the superlattice reflections belong to γ' and γ'' precipitates. Thus, the $(\bar{1}10)\gamma''$ spot also belongs to the $\{110\}\gamma'$ reflection. The mean size of the γ'' precipitates is about 30 nm. The orientation relationships between the γ matrix and γ'' precipitates are as follows:

$$\{112\}\gamma''\|\{111\}\gamma$$
$$\langle 1\bar{1}0\rangle\gamma''\|\langle 1\bar{1}0\rangle\gamma\,.$$

The bright-field observation of another area of this same specimen with a great magnification makes the following points clear (Fig. 10): (i) the γ'' precipitates are always revealed by a long double-lobe contrast (see A). (ii) The γ' precipitates may be separate, as shown in D; they are quasi-perfectly spherical. But, often, we note that they are coupled with γ'' small plates, along one of their faces (see C).

The contrast observed here in the case of the γ'' precipitates is similar to the one pointed out by Bourgeot, Faivre, *et al.*[9] in the case of an austenitic alloy Fe–30Ni–5Nb, in which tetragonal precipitates, which they have called γ*, have been formed during a tempering for 16 h at 650 °C.

For isothermal agings at 816 and 648 °C, respectively, made by Burger *et al.*[10] on Inconel 718 alloy, either the γ'' precipitates are first formed, or γ' and γ'' phases precipitate simultaneously. Besides, these authors point out that the γ' phase is never formed before γ''. At the opposite, for Radavich and Basile[3] the question (which among γ' and γ'' phases first precipitates for $\theta \leqslant 650$ °C) is still open. Thus, Cozar and Pineau[19] showed that the precipitation of the γ' phase precedes that of the γ'' phase for a value of the Ti + Al/Nb ratio higher than 0.8. Radavich[11] has also shown that the precipitation of γ' and γ'' phases would depend on the amount of Nb, time, and temperature of aging. In the present work, we have first observed the γ' precipitation in the case of a 4 h/680 °C aging and that for a value of the ratio Ti + Al/Nb = 0.71 only; then only after the 50 h/680 °C, the γ'' phase precipitation. As the amount of Nb was fixed in the alloy under consideration, the

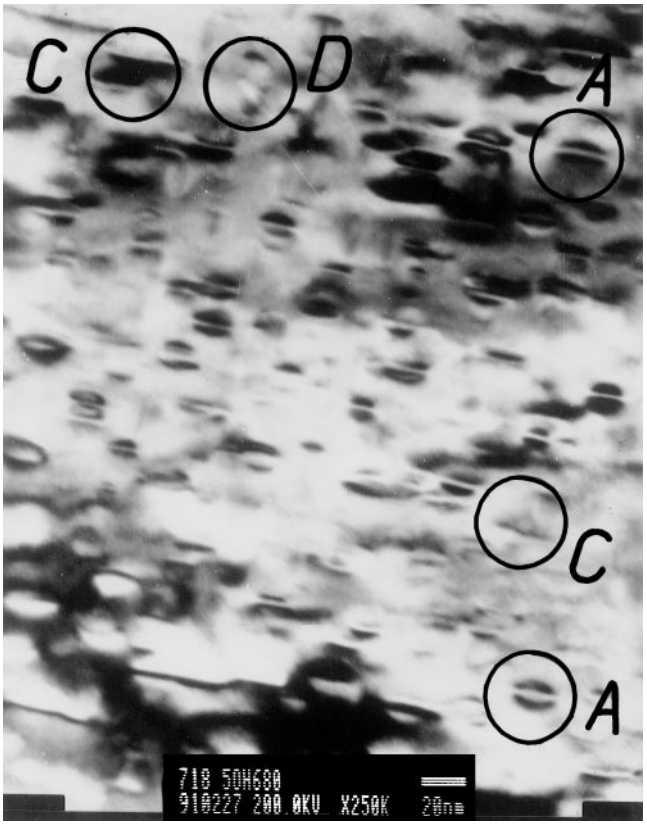

FIG. 10. Tempering for 50 h at 680 °C showing γ'' coherent precipitates with the matrix and γ' partially coherent precipitates.

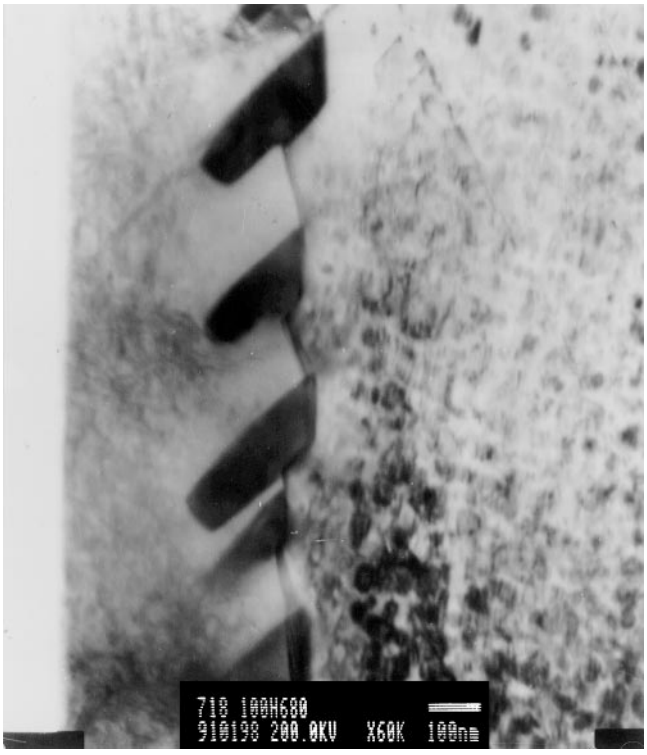

FIG. 11. Alloy aged at 680 °C for 100 h showing the growing of the β platelets and the presence of the γ'' denuded zone near the precipitates.

precipitation of either the γ' or γ'' will depend only on the temperature and the time of aging. In fact, for 550 and 600 °C, we show that the hardening is related to the γ' phase precipitation at least up to 100 h of aging. At 680 °C, for a 4 h aging, there is likewise a precipitation of the γ' phase; at the opposite, beyond this duration and for this same temperature, the resulting hardness is due to the γ'' phase precipitation.

After 100 h/680 °C of aging, Fig. 11 shows the β platelets are formed at the grain boundaries which are 0.26 μm sized and are parallel between them in one of the grains. The growing of these β lamellar precipitates in this grain creates a γ'' free zone in the interlamellar spaces and all along the grain boundary. This free zone has been previously observed by different authors[5,6–12]; x-microanalysis results obtained on the area shown in Fig. 11 are given in Table II. From these results, we may note that the chemical composition of (γ + γ'') is rather similar to that corresponding to the composition of the alloy itself (this being due to the small size of γ''). Furthermore, it is well known that the Nb amount in β phase is much more important than in (γ + γ'') (this being 18.52 against 7.55 wt.%). On the contrary, the analysis done between two β plates (i.e., in the free zone) shows a significant decrease in the Nb amount, which is in this case less than 3.96 wt.%. This fact confirms that the β precipitate growth in the γ grain takes place at the expense of the γ'' precipitates by

TABLE II. Chemical composition of some phases formed in Inconel 718 after aging at 680 °C for 100 h.

	Composition (%)	Ni	Fe	Cr	Nb	Ti	Mo	Al
γ'' precipitates and γ contribution	at.%	50.81	19.01	19.60	4.82	1.01	3.37	1.39
	wt.%	50.48	17.92	17.16	7.55	0.81	5.45	0.63
β precipitates	at.%	56.40	13.47	12.33	12.39	2.75	2.05	0.61
	wt.%	53.49	12.13	10.31	18.52	2.12	3.17	0.26
Denuded zone between two β plates	at.%	50.33	21.82	21.44	2.50	1.07	2.84	0.03
	wt.%	50.66	20.84	19.00	3.96	0.88	4.65	0.01

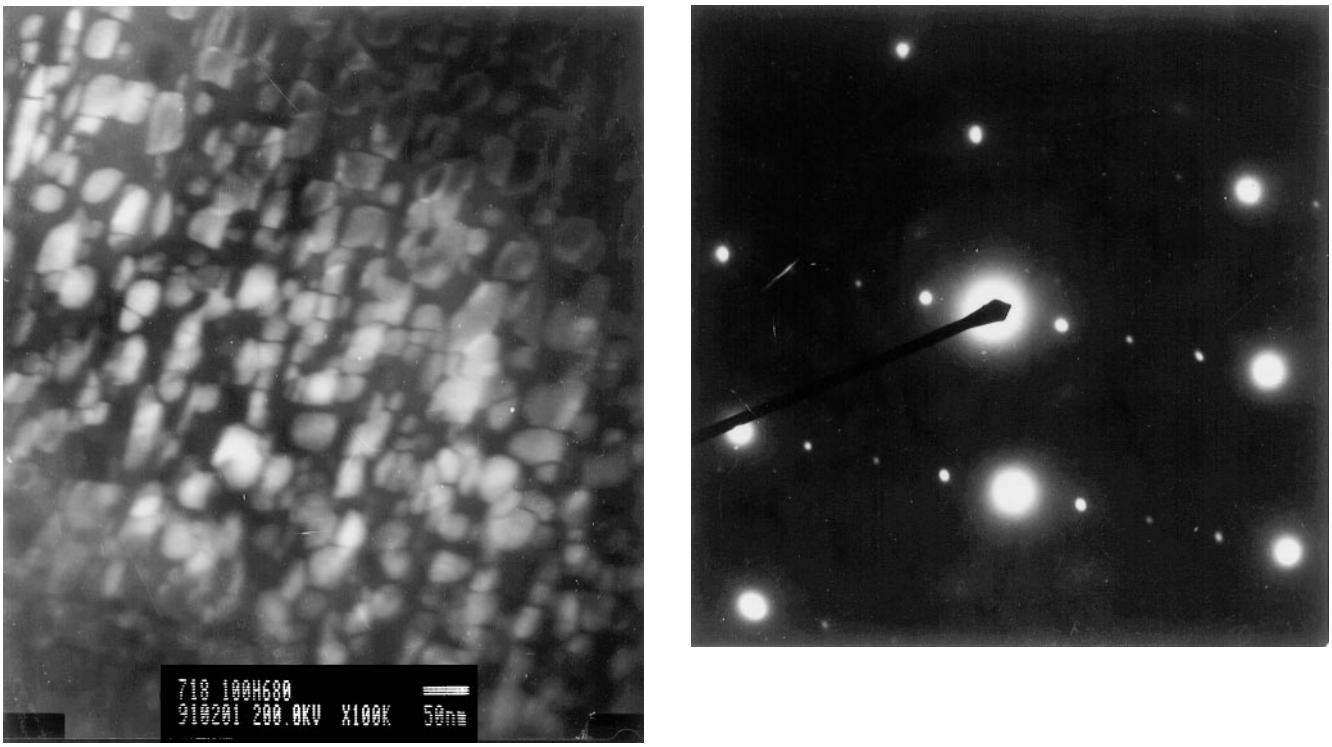

FIG. 12. Heat-treated 100 h at 680 °C: (a) dark-field image realized from $(\bar{1}0\bar{1})\gamma''$ spot and (b, c) electron diffraction pattern showing that the $\langle 22\bar{1}\rangle\gamma$ and $\langle\bar{1}10\rangle\gamma''$ zone axes are parallel.

capturing Nb, so it becomes a local formation of a γ'' depleted zone near the γ boundary. This behavior is consistent with the observations of Burke and Miller[13] who have shown that such a free zone is an indication of the Nb depletion adjacent to the β precipitates.

Dark-field examination done from the $(\bar{1}0\bar{1})\gamma''$ spot shows (Fig. 12) that γ'' particles have coarsened in such a way that they joined each other longitudinally which causes new interfaces; in some cases, parallel γ'' platelet systems have joined together. These γ'' precipitates are

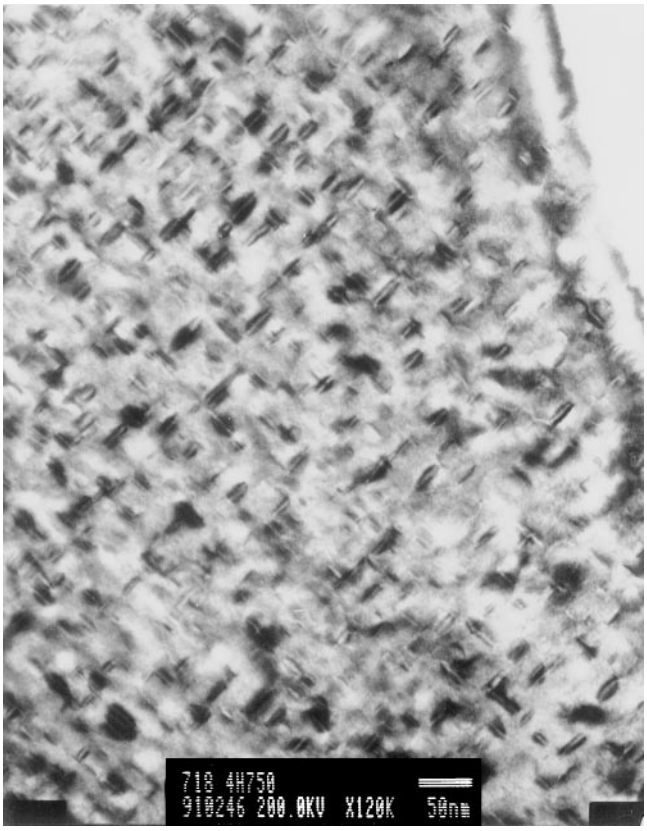

(a)

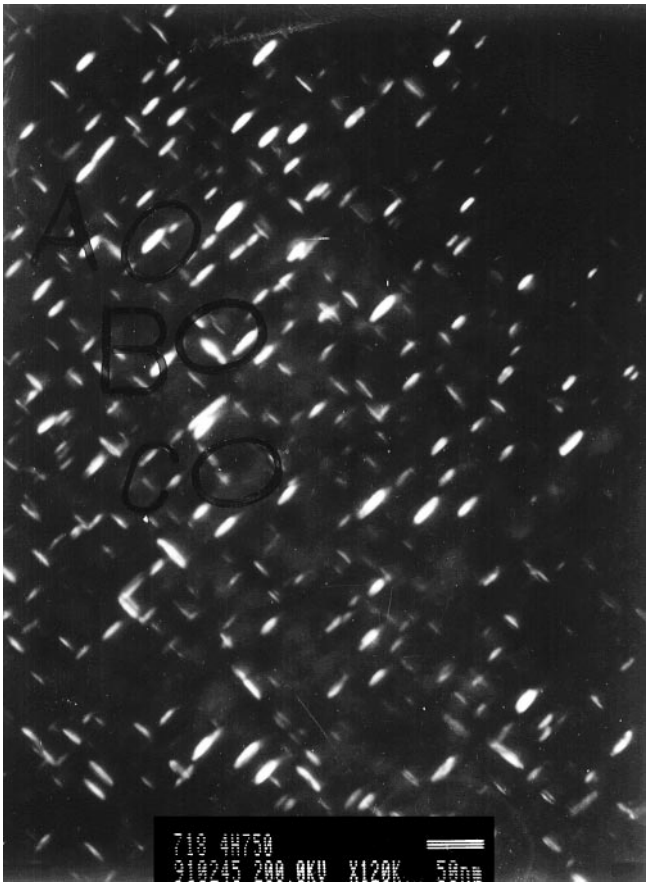

(b)

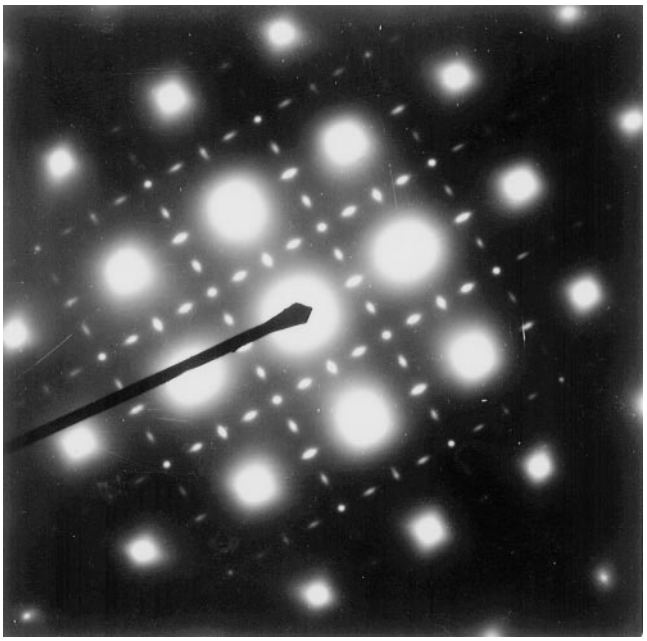

(c)

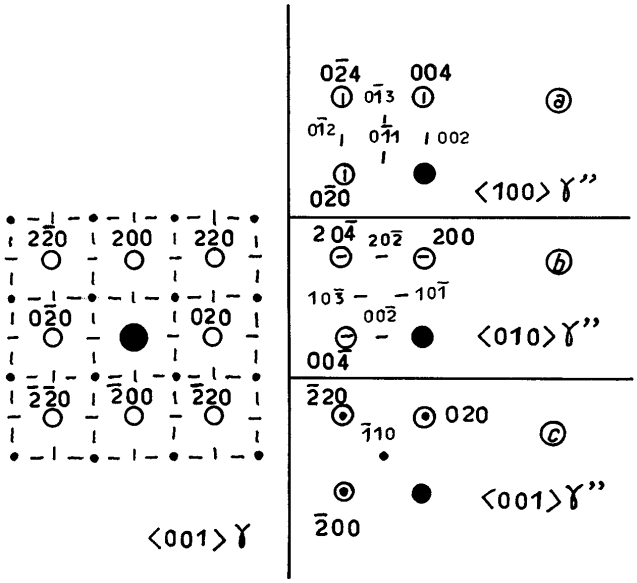

(d)

FIG. 13. Tempering for 4 h at 750 °C: (a) bright-field microscopy showing γ'' coherent precipitates, (b) dark-field microscopy showing the morphology of γ'' and γ' phases, and (c, d) electron diffraction pattern revealing the presence of three different variants of γ'' precipitates parallel to $\{100\}\gamma$.

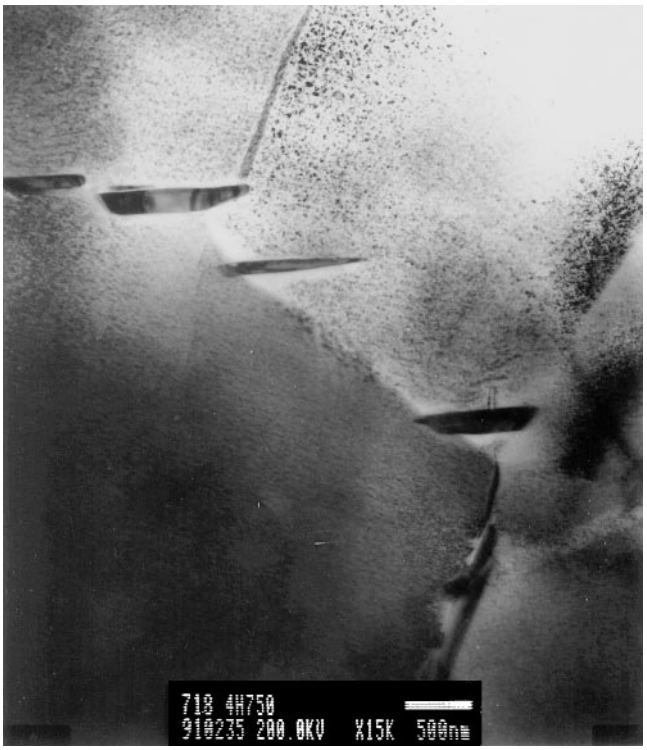

FIG. 14. Growth of the β platelets inside the γ grains at the expense of the γ'' precipitates.

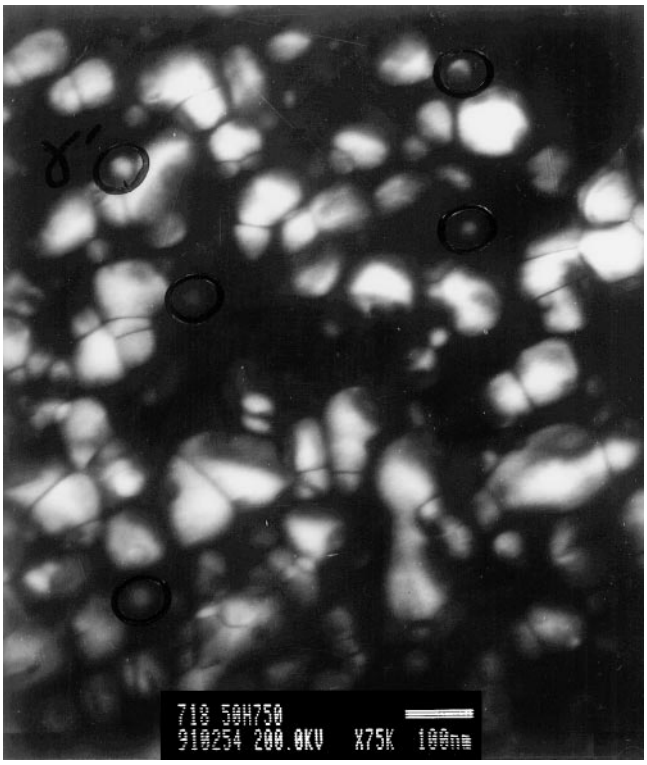

FIG. 15. Dark-field micrograph showing the precipitation morphology at 750 °C for 50 h.

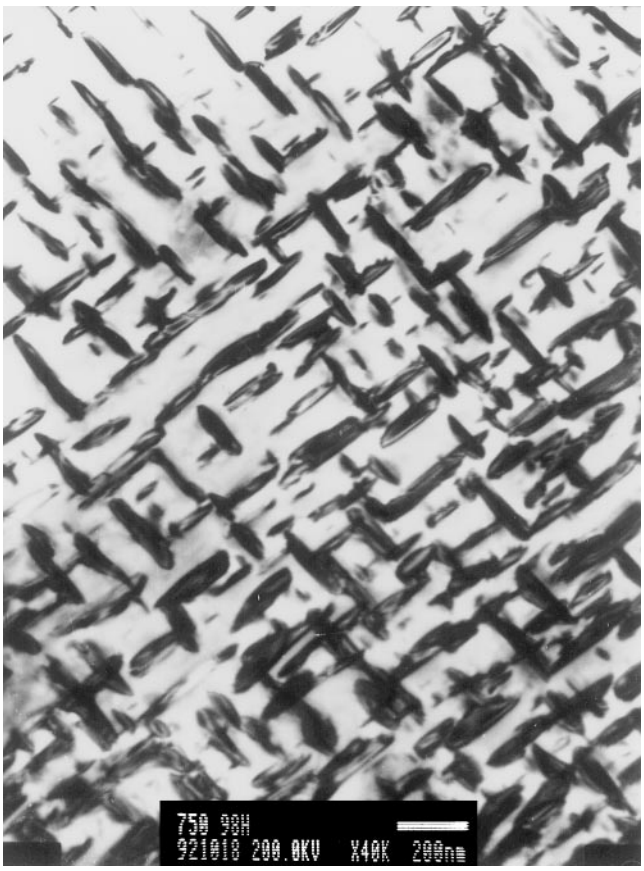

FIG. 16. Precipitation of the γ'' platelets at 750 °C for 98 h (bright field).

approximately 50 nm in size. The orientation relationships between the γ matrix and γ'' precipitates have been found to be:

$$(220)\gamma'' \| (220)\gamma$$
$$\langle \bar{1}11\rangle \gamma'' \| \langle 2\bar{2}1\rangle \gamma \,. \qquad (4)$$

Aging at 750 °C

After aging for 4 h at 750 °C, the bright-field micrograph shows the precipitation of the γ'' plates perfectly coherent with the matrix [Fig. 13(a)], presenting an elongated double-lobe contrast. In dark field, these γ'' precipitates appear as long disk-shaped, corresponding to three different variants [Fig. 13(b)]; the average size of the disk is 30 nm.

We note here the presence of spherical shaped γ' particles; usually, these γ' precipitates appear dark and are pinned on γ'' plates (see A, B, C). The diffraction pattern [Fig. 13(c)] shows superlattice reflections belonging, respectively, to γ' and γ'' precipitates. Figure 14 shows the growth of β platelets inside γ grains.

Figure 15 illustrates the change in shape of γ'' precipitates when they coarsen during a tempering at 750 °C for 50 h. Dark-field observation shows that γ'' precipitates have grown until they meet each other (thus creating new interfaces), resulting in globular and/or cuboidal particles. The average size of these particles is 80 nm. Yet, it is necessary to note the presence of the γ' precipitates (circled) which are almost perfectly spherical, and are distinct or associated with γ'' particles.

If the tempering duration is increased up to 98 h/750 °C, γ'' precipitates are as thin platelets (Fig. 16), their mean size now being 190 nm. Besides, for longer aging times at this temperature, the β equilibrium precipitates form at the expense of the metastable γ'' precipitates which are progressively dissolved [Fig. 17(a)]; only a few γ' spherical precipitates remain between β platelets. When γ'' precipitates vanish to favor β platelet growth, a γ'' denuded zone adjacent to the γ boundary appears, this zone being about 0.4 μm in width [Fig. 17(b)]. Similar results have been observed by Burke and Miller.[13]

3. Lattice parameters and γ'' particle shapes

The lattice parameters of the matrix and precipitates were measured by x-ray diffraction on extraction residues. Only the patterns corresponding to treatments carried out at 680 °C for 4 h, 50 h, and 98 h are given in Fig. 18.

We shall note that the two peaks at low θ angle as well as the peak between $\{111\}(Nb,Ti)C$ and $(002)\beta$ peaks are derived from the millipore filter. Whatever the time of tempering at 680 °C, all diffraction lines observed are similar, except after the 4 h treatment for which the pattern shows supplementary peaks associated with the γ' phase: {111}, {211}, and {220}.

Coherency strains (ϵ) were calculated according to the formalism proposed by Pineau and Cozar.[12,14] ϵ_{ij}^{T} being the strain tensor when changing from the fcc

(a)

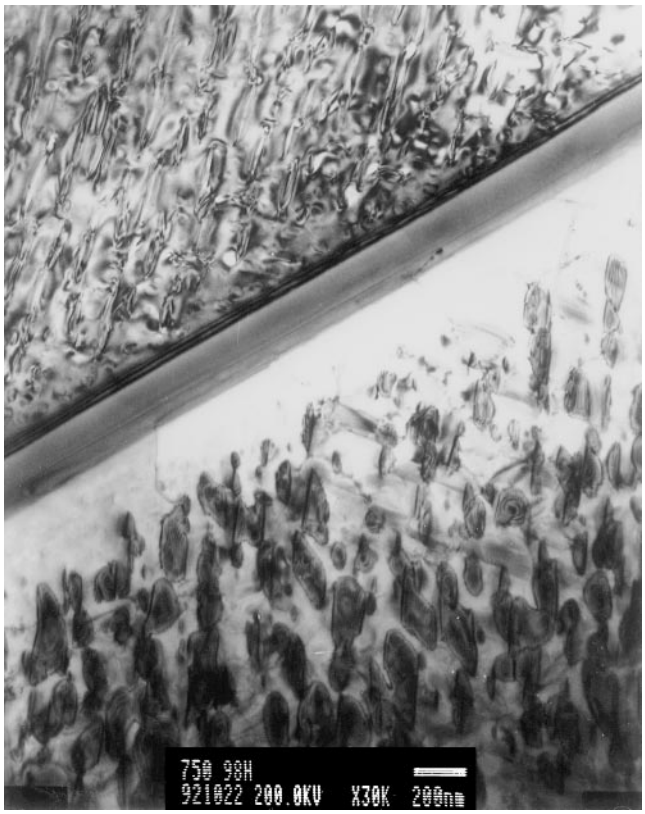

(b)

FIG. 17. Tempering for 98 h at 750 °C: (a) growth of the β platelets from the grain boundary (bright field) and (b) γ'' denuded zone near the γ boundary (bright field).

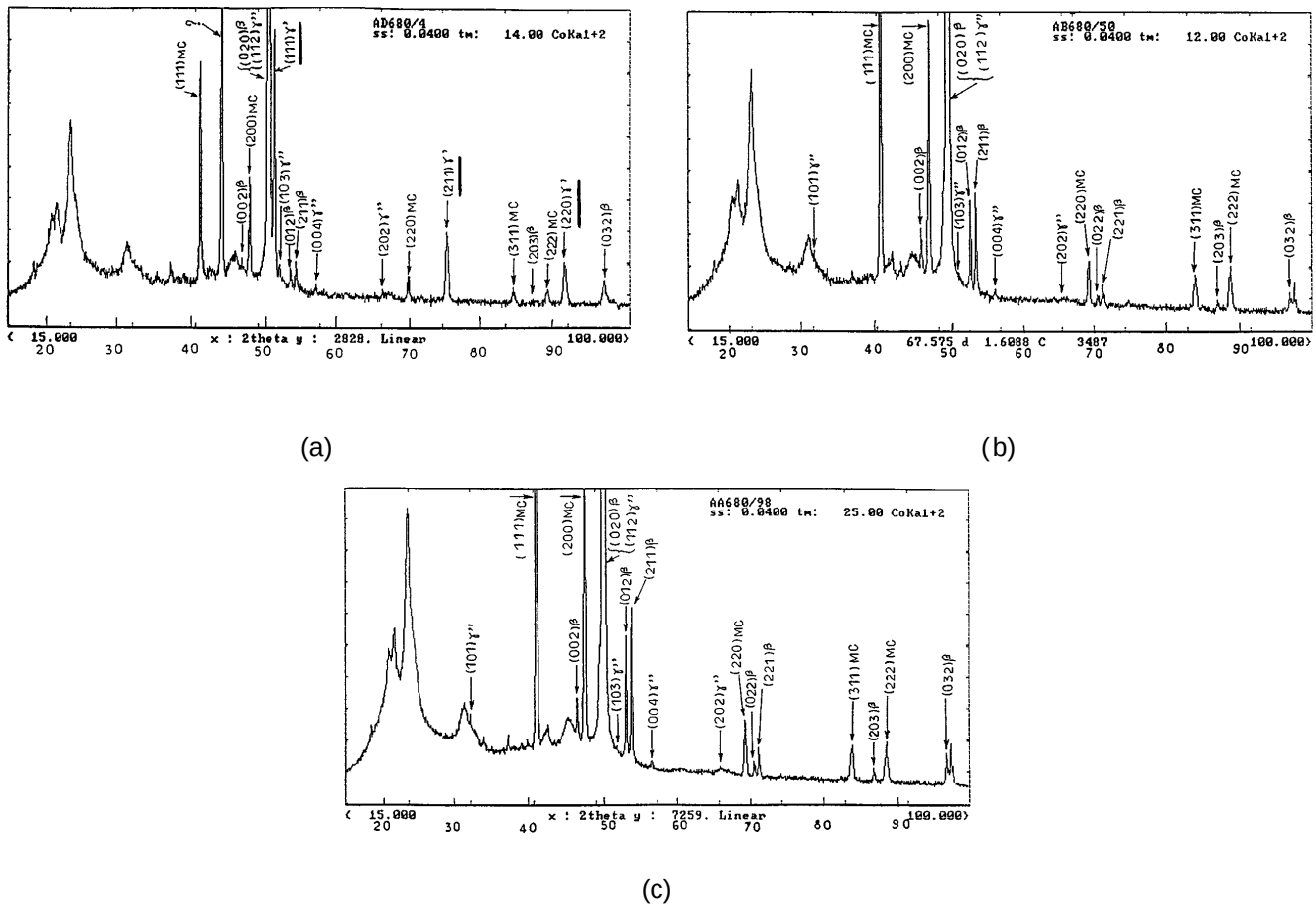

(a) (b)

(c)

FIG. 18. X-ray diffraction patterns registered by using the Co K_α radiation from the extraction residues at 990 °C for 30 nm and aged at 680 °C for (a) 4 h, (b) 50 h, and (c) 98 h.

relaxed cell of the matrix to the bct relaxed cell of the γ'' precipitate, one can write:

$$\epsilon_{ij}^{T} = \begin{pmatrix} \epsilon_{11}^{T} & 0 & 0 \\ 0 & \epsilon_{22}^{T} & 0 \\ 0 & 0 & \epsilon_{33}^{T} \end{pmatrix}$$

with

$$\epsilon_{11}^{T} = \epsilon_{22}^{T} = \frac{a_{\gamma''} - a_{\gamma}}{a_{\gamma}};$$

$$\epsilon_{33}^{T} = \frac{\frac{c}{2}(\gamma'') - a_{\gamma}}{a_{\gamma}},$$

which leads to

$$\epsilon_{\gamma-\gamma'}^{T} = \frac{a_{\gamma'} - a_{\gamma}}{a_{\gamma}}; \qquad \epsilon_{\gamma'-\gamma''}^{T} = \frac{a_{\gamma''} - a_{\gamma'}}{a_{\gamma'}}.$$

a_γ: parameter of the matrix as relaxed.
a_γ'' and $c_{\gamma''}$: parameters of γ'' as relaxed (extracted precipitates).
$a_{\gamma'}$: parameter of γ' as relaxed.

The resulting lattice parameters and coherency strains (misfits) are listed in Table III. We can note that parameters of the γ'' phase change as a function of the tempering duration, and the resulting variations modify especially the $(c/a)\gamma''$ ratio. The values of $a_{\gamma''}$ and $c_{\gamma''}$ after tempering at 680 °C or 750 °C (4 h) are consistent with those reported by Wagner and Hall[15] for this phase in Inconel 718 alloy, i.e., $a_{\gamma''} = 3.624$ Å, $c_{\gamma''} = 7.406$ Å, and $c/a = 2.044$.

Furthermore, the mismatch parameters are all lower than 1% in the $\langle 100\rangle\gamma''$ direction and are about 3% in the $\langle 001\rangle\gamma''$ direction. Our results are in good agreement with those reported by Cozar[12] for γ'' in Inconel 718. We will note also, according to results in Table III, that the relative importance of coherency strain value is as follows:

$$\epsilon_{\gamma-\gamma'} < \epsilon_{\gamma'-\gamma''} < \epsilon_{\gamma-\gamma''}.$$

According to Cozar,[12] the fact that the coherence deformation γ'/γ is much lower than that of γ''/γ will enhance the γ' nucleation, and consequently it will appear before the γ'' phase.

TABLE III. Values of lattice parameters and coherency strains (misfits).

Heat treatments	Lattice parameters (Å)	Coherency strains (ϵ)
990 °C/30 nm/W.Q. (1)	$a_{0\gamma} = 3.600 \pm 0.006$	
(1) + 680 °C/4 h/W.Q.	$a_\gamma = 3.596 \pm 0.006$ $a_{\gamma''} = 3.625 \pm 0.009$ $c_{\gamma''} = 7.410 \pm 0.018$ $(c/a)\gamma'' = 2.044 \pm 0.010$ $a_{\gamma'} = 3.603 \pm 0.006$	$\gamma - \gamma'' \longrightarrow \begin{cases} \epsilon_{11}^T = 0.0080 \\ \epsilon_{33}^T = 0.0303 \end{cases}$ $\gamma - \gamma' \longrightarrow \epsilon_{11}^T = 0.0019$ $\gamma' - \gamma'' \longrightarrow \epsilon_{11}^T = 0.0061$
(1) + 680 °C/50 h/W.Q.	$a_\gamma = 3.594 \pm 0.006$ $a_{\gamma''} = 3.609 \pm 0.008$ $c_{\gamma''} = 7.420 \pm 0.016$ $(c/a)\gamma'' = 2.055 \pm 0.009$	$\gamma - \gamma'' \longrightarrow \begin{cases} \epsilon_{11}^T = 0.0042 \\ \epsilon_{33}^T = 0.0323 \end{cases}$
(1) + 680 °C/98 h/W.Q.	$a_\gamma = 3.593 \pm 0.007$ $a_{\gamma''} = 3.605 \pm 0.008$ $c_{\gamma''} = 7.457 \pm 0.016$ $(c/a)\gamma'' = 2.068 \pm 0.009$	$\gamma - \gamma'' \longrightarrow \begin{cases} \epsilon_{11}^T = 0.0033 \\ \epsilon_{33}^T = 0.0377 \end{cases}$
(1) + 750 °C/4 h/W.Q.	$a_\gamma = 3.598 \pm 0.005$ $a_{\gamma''} = 3.630 \pm 0.006$ $c_{\gamma''} = 7.409 \pm 0.011$ $(c/a)\gamma'' = 2.041 \pm 0.006$ $a_{\gamma'} = 3.608 \pm 0.004$	$\gamma - \gamma'' \longrightarrow \begin{cases} \epsilon_{11}^T = 0.0089 \\ \epsilon_{33}^T = 0.0296 \end{cases}$ $\gamma - \gamma' \longrightarrow \epsilon_{11}^T = 0.0028$ $\gamma' - \gamma'' \longrightarrow \epsilon_{11}^T = 0.0061$
(1) + 750 °C/50 h/W.Q.	$a_\gamma = 3.596 \pm 0.005$ $a_{\gamma''} = 3.609 \pm 0.008$ $c_{\gamma''} = 7.423 \pm 0.016$ $(c/a)\gamma'' = 2.056 \pm 0.009$ $a_{\gamma'} = 3.599 \pm 0.005$	$\gamma - \gamma'' \longrightarrow \begin{cases} \epsilon_{11}^T = 0.0036 \\ \epsilon_{33}^T = 0.0321 \end{cases}$ $\gamma - \gamma' \longrightarrow \epsilon_{11}^T = 0.0008$ $\gamma' - \gamma'' \longrightarrow \epsilon_{11}^T = 0.0028$
(1) + 750 °C/98 h/W.Q.	$a_\gamma = 3.595 \pm 0.006$ $a_{\gamma''} = 3.606 \pm 0.007$ $c_{\gamma''} = 7.428 \pm 0.015$ $(c/a)\gamma'' = 2.059 \pm 0.008$	$\gamma - \gamma'' \longrightarrow \begin{cases} \epsilon_{11}^T = 0.0030 \\ \epsilon_{33}^T = 0.0331 \end{cases}$

In their study of γ' phase formation in the austenitic matrix, Hagel and Beattie[16] have suggested that nucleation of coherent precipitates is possible only if the coherence deformation ϵ_{11}^T is less than 1%. Thus our experimental results are in good agreement with the predictions of these authors.

The size (L) and thickness (e) of γ'' particles were determined from electron microscopy using the dark-field technique (each value corresponds to the average of measurements done on about 20 particles), with values being given in Table IV.

TABLE IV. Size (L) and thickness (e) of the γ'' particles at 680 °C and 750 °C.

	Time (h)	e (Å)	L (Å)	e/L
680 °C	50	100	300	0.333
	100	145	800	0.181
750 °C	4	90	300	0.3
	50	150	800	0.187
	98	340	1900	0.178

Some experimental points are displayed in Fig. 19 which shows the change in (e/L) ratio as a function of L in the case of Inconel 718, aged either at 680 or 750 °C for different times. On Fig. 19 we have also drawn theoretical curves according to Cozar[12] and Faivre,[17] relative, respectively, to Inconel 718 and Fe–30Ni–5Nb alloys for the change in (e/L) of γ'' as a function of L. These authors have used the same assumptions to make their calculations. The precipitates and the matrix are supposed to have the same elastic constants, which are assumed to be isotropic.

Cozar has considered an oblate spheroid shape for the γ'' platelets, whereas Faivre has supposed γ'' particles having a parallelepiped shape. It will be noted that our experimental points are correctly placed on the theoretical curve calculated by Cozar (Fig. 19, curve 1) and this up to a particle size of about 100 nm. Beyond

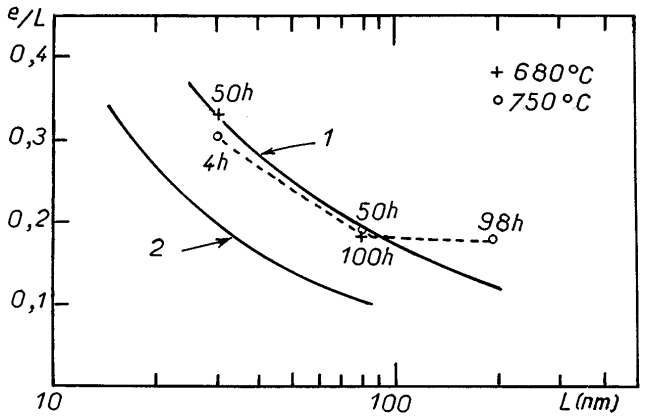

FIG. 19. Variation of (e/L) ratio as a function of size (L) for the γ'' phases. (1) and (2) are the theoretical curves according, respectively, to Cozar and Faivre.

this value the (e/L) ratio is rather independent of L. The point corresponding to (750 °C/98 h) is not on the curve calculated by Cozar, this fact being due to the loss of coherency for γ''. Similar results have been observed by Cozar and Pineau[14] in the case of Fe–30, 8Ni–9, 1Ta alloy, in which tetragonal γ'' precipitates become incoherent when they reach a size bigger than 120 nm. The (e/L) ratio decreases as L increases; consequently, γ'' precipitates have a tendency to flatten as a function of the tempering duration.

IV. CONCLUSION

This structural study of Inconel 718 alloy during treatments of tempering leads to the following conclusions:

(1) Changes in hardness, during isochronal tempering applied to the material previously quenched from 990 °C, are due to the precipitation of β, γ', and γ'' phases. When the tempering temperature is between 500 and 600 °C, β phase precipitates at the grain boundaries. Between 600 and 650 °C, an increase in hardness (HV = 350) is observed linked to the γ' phase precipitation. Between 650 and 750 °C an important γ'' phase precipitation occurs, which gives a noticeable increase in hardness (HV = 466). For temperatures higher than 750 °C, γ'' phase dissolution takes place while β phase forms, giving a progressive decrease in hardness (HV = 280 after treatment at 850 °C).

(2) TEM observations on thin foils have led to the identification of the different phases responsible for the various hardening stages occurring during isothermal tempering performed in the 500–750 °C temperature range from 1 to 100 h. γ' and γ'' phase precipitations are strongly dependent on the aging temperature and time. For temperatures lower than or equal to 600 °C, the observed hardening seems to be related to the γ' phase precipitation (very fine precipitates), at least up to a 100 h treatment duration. At 680 °C and for a value of the ratio Ti + Al/Nb = 0.71, the nucleation of the γ' phase is easier than that of the γ'' phase. The γ' phase first forms as confirmed by x-ray diffraction experiments. In fact, a first hardening (HV = 450) occurs when the duration is less than 4 h, which has been related to spherical shaped γ' precipitates. The γ' particle size is about 5–6 nm. Then a second hardening occurs between 4 and 50 h, with the maximum hardness reaching HV = 500. It corresponds to the precipitation of γ'' phase perfectly coherent with the γ matrix. In bright field, these γ'' precipitates present a double-lobe contrast. Also noted is the presence of γ' preciptates which are perfectly spherical and separate or pinned on γ'' particles.

At 750 °C, the γ'' phase precipitation (coherent with the matrix and disk-shaped with a diameter of 30 nm) produces a fast hardening since after a 4 h treatment the hardness is 466. For a longer thermal exposure (98 h) the γ'' platelets coarsen, then progressively dissolve while orthorhombic β phase ($D0_a$ type) appears. At this stage of tempering, γ'' precipitates have a mean size of 190 nm and they present no more fringe of double-lobe type contrast, this showing a loss of coherency.

(3) All the mismatch values are less than 1% along $\langle 100\rangle\gamma''$ and $\langle 010\rangle\gamma''$ and about 3% in the $\langle 001\rangle\gamma''$ directions. These ϵ values justify that γ'' particles grow as platelets, the more oblate as their size increases. These γ'' precipitates are still in coherency with the matrix until they reach about 100 nm.

REFERENCES

1. D. F. Paulonis, J. M. Oblak, and D. S. Duvall, Trans. ASM **62**, 611–622 (1969).
2. C. Slama, Thèse de Doctorat en Science, Université de Paris-Sud, Centre d'Orsay, 1993.
3. A. O. Basile and J. F. Radavich, *Superalloys 718, 625 and Various Derivatives* (The Minerals, Metals & Materials Society, Warrendale, PA, 1991), pp. 325–335.
4. A. E. Marsh, Metallurgia, 10–20 (1982).
5. I. Kirman, J. Iron and Steel Inst. **207**, 1612–1618 (1969).
6. M. Sundararaman, P. Mukhopadhyay, and S. Banerjee, Metall. Trans. **19A**, 453–465 (1988).
7. K. N. Tu and D. Turnbull, Acta Metall. **15**, 369 (1967).
8. K. N. Tu and D. Turnbull, Acta Metall. **17**, 1263 (1967).
9. J. Bourgeot, G. Faivre, J. Manenc, and D. Thivellier, Mém. Scient. Rev. Mét. **LXVI**, N°11, 845 (1969).
10. J. L. Burger, R. R. Biederman, and W. H. Courts, *Superalloy 718–Metallurgy and Applications* (The Minerals, Metals & Materials Society, Warrendale, PA, 1989), pp. 207–217.
11. J. F. Radavich, *Superalloy 718–Metallurgy and Applications* (The Minerals, Metals & Materials Society, Warrendale, PA, 1989), pp. 229–240.

12. R. Cozar, Thèse de Docteur-Ingénieur, Université de Nancy 1, 1973.
13. M. G. Burke and M. K. Miller, *Superalloys 718, 625 and Various Derivatives* (The Minerals, Metals & Materials Society, Warrendale, PA, 1991), pp. 337–350.
14. R. Cozar and A. Pineau, Scripta Metall. **7**, 851 (1973).
15. H. J. Wagner and A. M. Hall, DMIC; 217 (1965).
16. W. C. Hagel and H. Beattie, *Precipitation Processes in Steels* (Iron & Steel Inst., London, 1959), p. 98.
17. G. Faivre, Thèse de Docteur 3ème Cycle, Faculté des Sciences d'orsay, Université de Paris, 1969.
18. M. Sundararaman, P. Mukhopadhyay, and S. Banerjee, *Superalloys 718, 625, 706 and Various Derivatives*, edited by E. A. Loria (The Minerals, Metals & Materials Society, Warrendale, PA, 1994), pp. 419–440.
19. R. Cozar and A. Pineau, Metall. Trans. **4**, 47–59 (1973).